Radiologic changes in the aging nasal cavity*

Kimia G. Ganjaei[1,2], Zachary M. Soler[1], Elliott D. Mappus[1], Mitchell L. Worley[1], Nicholas R. Rowan[1], Guilherme J.M. Garcia[3], Lois J. Matthews[1], Judy R. Dubno[1], Mark A. Eckert[1], Rodney J. Schlosser[1]

[1] Department of Otolaryngology-Head and Neck Surgery, Medical University of South Carolina, Charleston, SC United States

[2] Rutgers Robert Wood Johnson Medical School, Piscataway, NJ United States

[3] Department of Otolaryngology and Communication Sciences, Medical College of Wisconsin, Milwaukee, WI, United States

Rhinology 57: 2, 117 - 124, 2019
https://doi.org/10.4193/Rhin18.096

***Received for publication:**
May 7, 2018
Accepted: August 13, 2018

Background: With an aging population, it is important to understand age-related anatomic changes in the nasal cavity and cribriform plate (CP) that may have clinical implications.

Methodology: Computed tomography (CT) scans obtained for non-rhinologic conditions were divided into a young cohort (N=35, 18-34 years old) and an older adult cohort (N=32, 80-99 years old). Intranasal airspace volumes and bony anatomy of the CP were manually segmented using OsiriX software. The CP was assessed for mean Hounsfield Units (HU) and percentage of olfactory foramina. Deformation based morphometry (DBM) was then performed on the same cohort and correlated with manual measurements.

Results: Individual nasal cavity volumes increased 17-75% with age. Regression analysis of all scans revealed age to be the predominant variable influencing intranasal volume differences when controlling for sex and head size. Mean HU of the CP negatively correlated with age. No age-related differences in bone stenosis of olfactory foramina were identified. Automated DBM measurements of intranasal volumes, as well as CP and zygoma mean HU correlated with manual measurements.

Conclusion: Older subjects have a global increase in intranasal volumes and diffuse bone density loss in the CP. The clinical impact of age-related anatomic changes in the nasal cavity and CP requires further investigation.

Key words: aging, airspace volume, cribriform plate, bone density, nasal, olfactory

Introduction

As the population ages, providers are treating an increasing number of older adult patients with various rhinologic disorders. Olfactory dysfunction and senile rhinitis are more prevalent in the older population. Other conditions, such as chronic rhinosinusitis, allergic rhinitis and non-allergic rhinitis also commonly afflict the elderly [1-6]. Understanding age-related anatomic changes in the nasal cavity and skull base will enable us to better understand and subsequently treat rhinologic conditions that occur in these patients. A variety of methods have been used to assess age related changes in nasal anatomy, including radiologic studies, rhinomanometry, and cadaver dissection [5,7,8, 10-12]. These studies have demonstrated increased overall nasal cavity volume, increased mean cross-sectional areas for airflow through anatomically narrow nasal regions, and stenosis of olfactory foramina [5,7,8,10-12]. Unfortunately, these studies require manual assessments of imaging studies, physiologic studies of airway anatomy, or autopsy investigations. These methods, while sufficient to measure age related differences, are also labour-intensive for investigators and patients and can be prone to error. Thus, reliable methods for rapidly assessing age-related anatomic changes were explored in this study. The goal of this study was to use non-invasive manual and automated techniques to comprehensively assess age-related changes in overall nasal anatomy and in specific nasal regions that have not yet been examined using computed tomography.

Materials and methods

Study population and CT selection

This study was a radiologic case-control study comparing an older cohort to a younger control population. CT scans were iden-

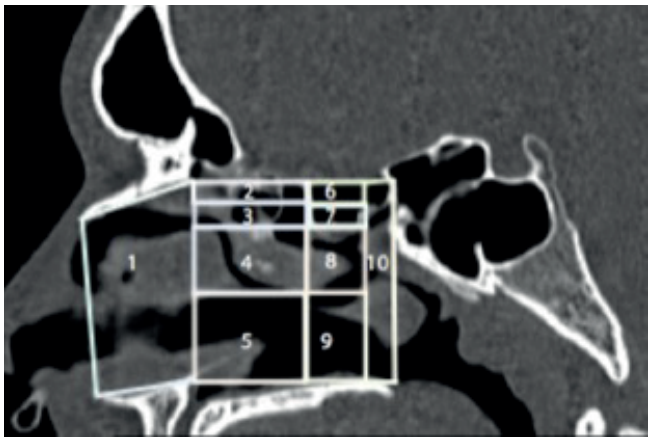

Figure 1. Individual volume of interest (VOI) regions 1-10 defined for intranasal volumes in the sagittal view, (1) pre-olfactory region from the nasal bone to anterior to the nasolacrimal duct, (2-5) the subdivided anterior olfactory cleft region, terminating at the end of the anterior ethmoid artery, (6-9) the subdivided posterior olfactory cleft region, terminated just anterior to the posterior ethmoid artery, (10) the nasopharynx, measurement terminating at the posterior vomer.

tified using institutional radiology logs to identify all patients who had previously received non-contrast axial head CTs with 0.6mm cuts that included the entire cribriform plate for non-rhinologic diagnoses. All scans were reviewed by a rhinologist, and patients were excluded if imaging revealed sinonasal disease, trauma, or anatomic abnormalities of the cribriform plate. CTs were selected based upon adequate quality and thoroughness of scan and then divided into young (18-34 years old) and old (80-99 years old) cohorts. Approval for this study was granted by the institutional review board of the Medical University of South Carolina (IRB#00066646.)

Manual segmentation

Nasal cavity airspace volumes: Digital Imaging and Communication in Medicine (DICOM) images were uploaded into OsiriX MD imaging software (Pixmeo, Bernex, Switzerland) [13]. Trained research personnel reviewed all scans, blinded to age and sex of patients. All measurements were recorded using OsiriX in the coronal plane using CT bone window (W:1500 L:300) with anatomic boundaries confirmed using linked sagittal and axial images. Volumes were measured using the 2D segmentation function in OsiriX measuring air pixels within the nasal cavity. A total of 10 volumes of interest (VOI) were measured in each scan, as shown in Figure 1. Volume 1 was the pre-olfactory VOI and extended from the nasal bone to the anterior border of the nasolacrimal duct. Volumes 2 through 5 were the anterior olfactory VOIs and were defined from the anterior border of the nasolacrimal duct to the anterior ethmoid artery (AEA). This anterior olfactory VOI was subdivided into independent VOIs from superior to inferior so that VOI 2 was the superior 5 mm beneath the cribriform plate, VOI 3 was 5-10 mm beneath the cribriform

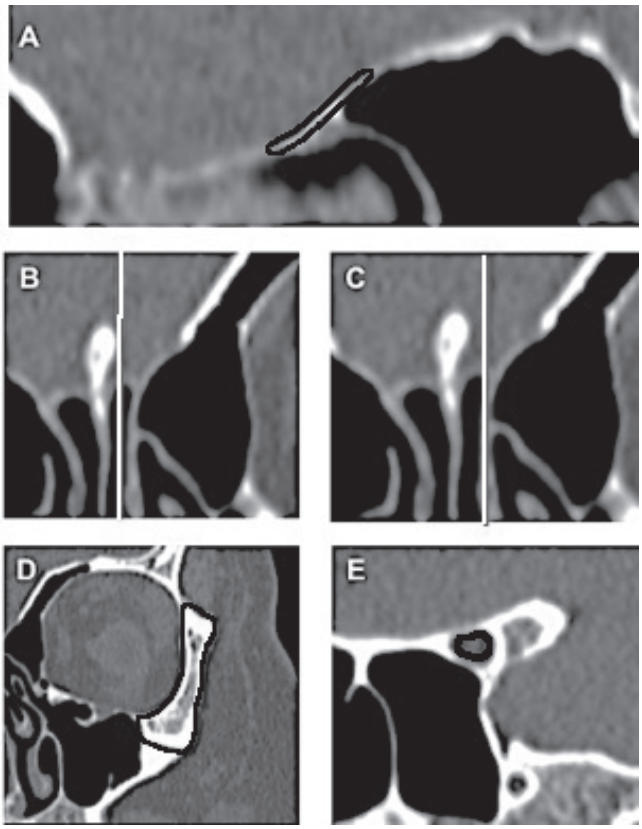

Figure 2. Samples of cribriform plate, zygomatic, and optic nerve measurements using OsiriX and manual segmentation. (A) One sagittal region of interest (ROI) of the cribriform plate, (B) Anterior-medial boundary of cribriform measurement, (C) Anterior-lateral boundary of the cribriform measurement, (D) Sample of left zygoma, (E) Sample of left optic nerve.

plate, VOI 4 extended down to the inferior border of the middle turbinate and VOI 5 extended from the inferior border of the middle turbinate to the inferior border of the inferior turbinate. Volumes 6 through 9 were the posterior olfactory VOIs, which extended from the AEA to the posterior ethmoid artery (PEA) as previously described [14]. This posterior olfactory VOI was then subdivided from superior to inferior into VOIs 6 through 9 in an identical fashion as described for the anterior olfactory VOIs. The post-olfactory VOI was VOI 10 and extended from the PEA to the posterior border of the vomer. Olfactory cleft volumes included the VOIs 2, 3 and 4 for the anterior portion and 6, 7 and 8 for the posterior portion. Given prior reports of the impact of sex upon airspace volumes, males and females within age cohorts were analysed separately.

Cribriform plate measurements: CT measurements of the CP were completed using OsiriX software as our group has previously described [14]. Briefly, we analysed a pre-defined segment of the posterior CP between the AEA and PEA to exclude confounding by the AEA and PEA foramina, which can be quite large [15]. Four sagittal slices of the CP were measured on the right and left of the crista galli as shown in Figure 2A-C. All sagittal measurements were drawn to a height of 0.6mm from the superior edge

of the cribriform to include all pixels encompassing this region. Using the plugin software pyOsiriX 1.0.1, the raw voxel data from each VOI was exported and recorded in Microsoft Excel [16]. When examining variability within each individual CP, anterior and posterior segments were designated as the volumetric region corresponding to the 4 most anterior and 4 most posterior voxels of the cribriform measurement. It should be noted that given our pre-defined sampling of the posterior segment of the CP, the anterior sample actually corresponds to the middle of the CP and will be referred to as such.

Olfactory Foramina Analysis: We used the left optic nerve as a surrogate measure for soft tissue/neural structures. A single area measurement was taken from the left optic nerve within the optic canal which can be seen at the level of the sphenoid sinus in the coronal view (Figure 2E). Bone was then defined as >2SD above soft tissue and air was defined as <2SD below soft tissue. The percentage of bone composition was calculated in each scan as previously described using two methods, the first method including all voxels and the second method excluding any voxels corresponding to air that should not be present in the CP [14].

Zygoma measurements: CT measurements of the zygomatic bone were used to determine if age-related changes in bone density in the CP occurred in isolation or in synchrony with bone density loss in other craniofacial bones. A single area measurement was measured of the left zygomatic arch (Figure 2D). This region of interest (ROI) was measured when the zygomatic frontal suture and zygomaxillary suture were both present on coronal view as previously described [17]. The raw pixel data from each scan were analysed as described for the CP.

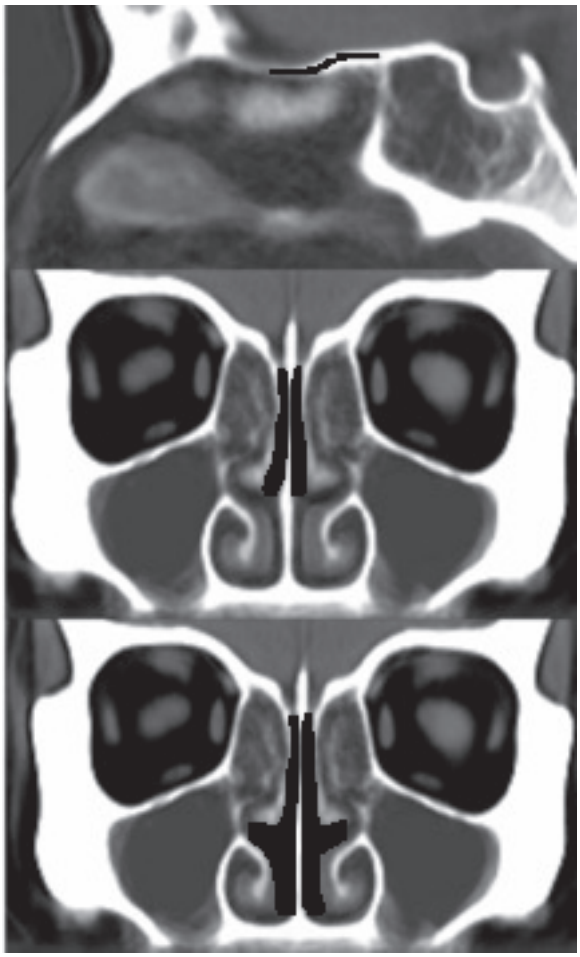

Figure 3. Volumes of interest (VOI) in the template space for automated CT measurements of (A) the cribriform plate, (B) olfactory cleft volume, and (C) total intranasal volume.

Automated segmentation

Imaging pre-processing for deformation-based morphometry (DBM): The DICOM images were uploaded to a secure server, de-identified, and converted to the Neuroimaging Informations Technology Initiative (NifTI) file format for analysis. Images were manually aligned, and a common origin was set at the midline anterior aspect of the sella turcica. The images were then rigidly aligned using SPM12 (Wellcome Department of Imaging Neuroscience Group, London, UK) and resliced to a 0.6 mm isotropic resolution (in the acquisition plane the images had a slice thickness 0.6 mm, but slice thickness varied across scans in the other two planes). The resliced images were thresholded at -250 Hounsfield units (HU) (setting voxels with HU < -250 equal to 0) to limit image artefacts posterior and superior to the skull as well as variation in air voxel densities from influencing the normalization procedure. The Advanced Normalization Tools (ANTS) diffeomorphic normalization was then run for 10 cycles using a cross-correlation cost function and the affine average of the thresholded images as the initial starting template. The thresholded images were then normalized into the final template space using the ANTS generated deformation fields.

Nasal cavity airspace volumes: Automated measures of airspace volumes were collected to establish measurement reliability and confirm findings from the manual measures. The olfactory cleft (OC) airspace extended from the cribriform plate superiorly and was bounded anteriorly by a plane through the nasolacrimal duct, and posteriorly by the face thickening of the skull base at the junction of the cribriform plate and planum. Medially it was bound by the septum and laterally it was bound by the middle turbinate and extended inferiorly to the lower border of the middle turbinate. The automated OC airspace approximated VOIs 2-4 and 6-8 from the manual measurements. The total intranasal volume VOI extended the olfactory cleft VOI inferiorly to the lower border of the inferior turbinate. This region approximated VOIs 2-9 from the manual measurements. The intranasal airspace VOIs were inverse warped into the individual subject non-thresholded CT scans using the ANTS generated deformation fields (Figure 3A-C). The volume of air voxels encompassed by each VOI were then summed using SPM12 as a volumetric measurement.

Table 1. Intranasal airspace volume differences by age group and sex using manual segmentation.

	Men			Women		
VOI	Mean ± SD in cm^3 Ages 18-34 (n=12)	Mean ± SD in cm^3 Ages 80-99 (n=11)	Mean percent difference with aging	Mean ± SD in cm^3 Ages 18-34 (n=15)	Mean ± SD in cm^3 Ages 80-99 (n=18)	Mean percent difference with aging
1	3.62 ± 0.75	5.26 ± 1.16	37%†	3.29 ± 1.01	5.14 ± 1.22	44% ††
2	0.15 ± 0.07	0.22 ± 0.07	38% †	0.22 ± 0.07	0.26 ± 0.06	17%
3	0.15 ± 0.08	0.21 ± 0.09	33%	0.19 ± 0.06	0.25 ± 0.09	27%
4	0.60 ± 0.22	0.98 ± 0.45	48% †	0.88 ± 0.42	1.32 ± 0.54	40% ††
5	0.87 ± 0.24	1.50 ± 0.55	53% †	0.82 ± 0.22	1.56 ± 0.83	62% ††
6	0.09 ± 0.06	0.12 ± 0.06	29%	0.11 ± 0.09	0.13 ± 0.04	17%
7	0.10 ± 0.06	0.13 ± 0.07	26%	0.10 ± 0.06	0.13 ± 0.04	26% ††
8	0.51 ± 0.19	0.79 ± 0.28	43% †	0.70 ± 0.30	1.05 ± 0.33	40% ††
9	0.42 ± 0.15	0.57 ± 0.22	30% †	0.43 ± 0.14	0.71 ± 0.26	49% ††
10	0.94 ± 0.66	2.07 ± 1.14	75% †	1.01 ± 0.84	1.91 ± 1.42	62%
AntOC	0.91 ± 0.29	1.41 ± 0.57	43% †	1.12 ± 0.43	1.72 ± 0.77	42% ††
PostOC	0.65 ± 0.26	1.05 ± 0.38	47% †	0.85 ± 0.37	1.32 ± 0.36	43% ††
TotOC	1.56 ± 0.54	2.45 ± 0.91	44% †	1.96 ± 0.67	3.04 ± 1.07	43% ††
TotVol	7.24 ± 0.99	11.95 ± 3.13	49% †	7.59 ± 1.93	12.07 ± 2.94	46% ††

VOI=volume of interest, AntOC=anterior olfactory cleft, PostOC=posterior olfactory cleft, TotOC=total olfactory cleft volume, TotVol=total volume of olfactory cleft, †Volumes with statistically significant mean differences at $p<0.05$, ††Volumes with statistically significant mean differences at $p<0.001$.

Cribriform plate measurements: The cribriform plate VOI extended from the face of the sphenoid anteriorly to the last coronal cut not including the globe. This approximates a sample of the CP between the AEA and PEA, similar to our manual segmentation. The HU values for each voxel in the cribriform plate ROI's were then extracted from the normalized images. CP bone density and olfactory foramina stenosis were then calculated as described above for manual segmentation.

Zygoma measurements: Zygoma ROI was outlined as described above for manual segmentation. Zygoma mean HU was then calculated based upon the automated voxel data.

Controlling for head size

Both manual and automated airspace volume measurements were corrected for head size. CT images were rigidly aligned using SPM12 (Wellcome Department of Imaging Neuroscience Group, London, UK). If a scan needed to be sampled outside of the original image for realignment due to bounding box differences at the time of CT acquisition, the HU values at these voxels were set at exactly 0 and these voxels were excluded from the head volume measurements. Three tissue types—bone, neural/soft tissue and air—were defined as previously described [14] with bone corresponding to >2 standard deviations (SD) above the mean HU of a soft tissue sample, and air <2 SD below this measure. Soft tissue was defined in the current study with the optic nerve as a surrogate measure for neural structures such as olfactory nerve filaments. A head size volume estimate was assessed by the number of voxels defined as bone. This avoids changes in soft tissue volumes that may occur with aging and changes in weight, rather than true changes in craniofacial skeleton.

Statistical analysis

Statistical analysis was performed using commercially available software applications (SPSS v24; IBM Corporation, Armonk, NY.) Descriptive statistics are reported using mean and SD where appropriate. Raw voxel data were used to obtain HU cribriform measurements. Independent 2-sided t-tests and percent difference calculation were used to compare intranasal airspace volumes by age and sex, mean HU for the total and regional cribriform as well as zygoma VOIs. Cohen's d test was used to calculate for effect size between age cohorts. Multivariate linear regression for all ages combined was used to analyse four different intranasal volumes previously shown to be relevant to olfactory function using models for age, sex, and head size as defined previously [7, 11, 18-20]. Cohen's f^2 was used to assess local effect size of age. Pearson and Spearman correlation coefficients were calculated for parametric and non-parametric data, respectively.

Results

Patient demographics and manual segmentation of airspace volumes

The young cohort consisted of 35 patients, mean age of 25.0 ±

Table 2. Multivariate regression analysis of intranasal volumes.

VOI	Model†	B	SE	t statistic	Sig	Cohen's f² ††
TotVol	Age	0.060	0.013	5.111	p<0.001	0.57
	Sex	-0.083	0.759	-0.112	p=0.911	
	Head size	-0.002	0.003	-0.874	p=0.387	
TotOC	Age	0.013	0.004	3.226	p=0.002	0.06
	Sex	0.404	0.236	1.710	p=0.093	
	Head size	-0.001	0.001	-1.026	p=0.310	
1	Age	0.031	0.006	5.557	p<0.001	0.67
	Sex	-0.110	0.322	-0.342	p=0.734	
	Head size	0.001	0.001	1.340	p=0.187	
4	Age	0.004	0.002	2.053	p=0.045	0.08
	Sex	0.239	0.122	1.964	p=0.055	
	Head size	-0.001	<0.001	-1.712	p=0.093	

VOI=Volume of Interest, TotVol=total intranasal volume, TotOC=total olfactory cleft volume, B=beta, SE=standard error, Sig=significance, † All models for head size volume measured in cm^3, †† Cohen's f^2 for age model.

Table 3. Manual segmentation of cribriform plate bone density and olfactory foramina.

		Bone density		Olfactory foramina stenosis	
Age group in years	Volume in mm^3, mean (SD)	CP HU mean (SD) †	Zygoma HU mean (SD)	Bone voxels / total voxels mean (SD)%	Bone voxels / (bone+soft tissue voxels) mean (SD)%
18-34	17.9 (3.3)	499.5 (153.1)	1098.1 (103.9)	83.3 (10.9)%	90.5 (6.8)%
80-99	17.5 (3.08)	381.5 (123.5)	922.9 (131.4)	84.0 (12.0)%	90.4 (7.1)%
Mean diff	0.41 (.78)	118.0 (34.2)	175.2 (30.8)	-0.7 (2.8)%	1.7 (-3.3)%
Sig	p=0.605	p=0.001	p<0.001	p=0.782	p=0.962
95% CI of diff	-1.1-2.0	49.7-186.3	113.6-23.9	-6.4-4.8%	-3.3-3.5%

SD=standard deviation, CP= cribriform plate, HU=Hounsfield units, Diff=difference Sig=significance

3.9 years. The older cohort consisted of 32 patients, mean age 89.0 ± 4.7 years. Of the 67 CT scans, 11 (8 young, 3 old) were unable to be used for airspace volumes as they did not encompass the entire nasal cavity and were cropped anteriorly or inferiorly. All airspace volumes were larger from 17% to 75% in older than younger patients for both males and females, as shown in Table 1. The largest group differences were seen in VOIs 5 and 10. Including both sexes, effect sizes were moderate to large except for VOI 6 (Cohen's d>0.5-0.8). We then used multivariate regression to examine total intranasal volume, total OC volume and selective VOIs (1 and 4) that have been reported to change with age and have potential clinical significance [9,11,19,20]. Multivariate regression analysis of all scans revealed that age was the only statistically significant variable in the model influencing intranasal total and olfactory cleft volumes as well as VOIs 1 and 4 (Table 2). Local effect size for age was largest for total intranasal volume and VOI 1 (Cohen's f2 =0.57 and 0.67, respectively).

Manual segmentation of cribriform plate

Of the 67 CT scans, 8 scans (6 young, 2 old) were unable to be used in zygomatic analysis because the entire zygomatic region was not visible on a single CT cut. Older subjects had significantly lower HU measurements for both the CP and the zygomatic bone (Table 3). Histogram of the raw pixel data of the CP using a random sample of 32 scans in each age cohort showed a loss in the number of high density bone voxels>700 HU in the older cohort with a corresponding increase in the number of low density bone voxels <400 HU (Figure 4A). This pattern was also evident with zygoma samples (data not shown). The mean HU of both the CP (r=-0.391, p <0.001) and zygoma (r=-0.584, p <0.001) negatively correlated with age. Mean HU of the zygoma correlated with the cribriform plate in all ages in (r=0.369, p =0.004). Regional differences were found in bone density of the CP. The anterior boundary of the measurements, which in our study corresponds to the middle portion of the cribriform plate just posterior to AEA, was significantly less dense than the posterior region in both age groups (Figure 4B). Effect sizes were large between age groups for mean cribriform HU (d=0.85), and zygoma mean HU (d=1.48). No difference in olfactory foramina stenosis was found using either method of assessment (Table 3).

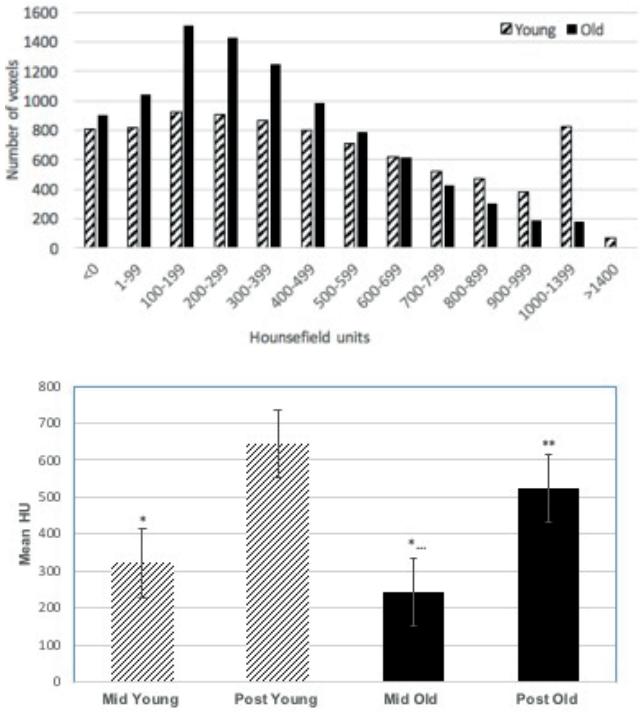

Figure 4. A.)Distribution of cribriform plate voxel values using manual segmentation. While overall number of bone voxels in the cribriform plate is constant between groups, note the higher number of voxels >700 HU in the young cohort, while the old cohort has an increase in number of voxels between 100 and 399 HU. B) Cribriform plate regional bone density differences using manual segmentation. *Middle regions had significantly lower mean HU than posterior regions in both age groups, p <0.001,**older patients had significantly lower mean HU than young patients in both middle and posterior regions, p <0.05. Mid = middle region, Post = posterior region, HU = Hounsfield Units.

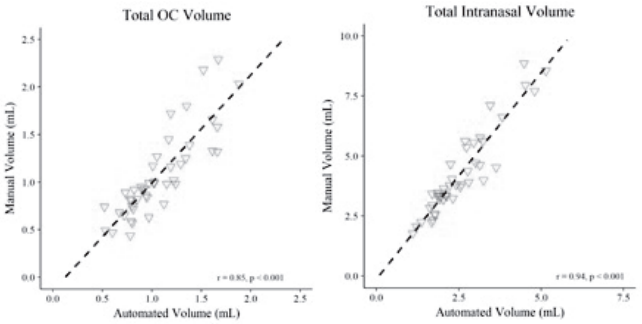

Figure 5. Correlation between manual and automated computed tomography (CT) measurements for total intranasal volume (R) and total olfactory cleft volume (L). OC= olfactory cleft.

Automated CT analysis

Twelve scans were excluded due to significant artefacts outside the head which could inhibit the normalization procedure leaving 47 scans for analysis (20 young, and 27 old). Automated measurements of intranasal volume were highly correlated with manual segmentation for total intranasal volume (r=0.94, p<0.001) and total olfactory cleft volumes (r=0.85, p<0.001 Figure 5). Automated measurements of the bone density (mean HU) of the cribriform plate, zygoma, and foraminal stenosis are also correlated as shown in Table 4.

Discussion

With an aging population, it is important to understand age-related anatomic changes that may impact a variety of rhinologic disorders. Using non-invasive radiographic methods, we identified several age-related changes in nasal cavity and cribriform plate anatomy. Manual segmentation techniques are labour-intensive and prone to error, thus we also confirmed use of a novel method for automated CT analysis. The results correlated with manual measurements and this technique offers greater efficiency for future imaging studies.

We found widespread increases in nasal cavity volumes associated with increased aging. Males and females shared a similar profile of changes with increased age across all volumes. Our study adds to the current literature with a comprehensive analysis of 10 intranasal regions supported by both manual and automated methods. Loftus et al. also used CT analysis to demonstrate increases in overall intranasal volume with age but did not examine age-related differences in specific intranasal volumetric subdivisions [11]. Acoustic rhinometry studies did demonstrate changes in specific cross-sectional areas with age, but rhinometry as a technique does not always correlate with exact anatomic landmarks [7,8]. Anatomic landmarks are important for establishing specific age-related changes in intranasal volumes. In addition, we analysed the impact of age, sex and head size on specific intranasal regions [7,8,11]. Age was found to be the predominate factor influencing intranasal volumes [11,19]. The older adult population is known to have atrophy of the nasal mucosa and loss of nasal structural integrity, which are thought to contribute to several clinical complaints including rhinorrhoea, dry mucus, and the paradoxical sensation of congestion [1,2,6]. Regardless of the mechanisms of mucosal atrophy, increased intranasal volumes in older adults are likely to impact nasal airflow patterns. Altered airflow has been hypothesized to impact subjective sensation of nasal obstruction and likely impacts local mucosal temperature gradients and mucus viscosity [9-11,19]. Another cause of nasal obstruction is nasal valve collapse. The nasal valve corresponds to the pre-olfactory region designated as VOI 1 in our study and we found a marked increase in these volumes with aging [5,20]. In addition to rhinitis and nasal obstruction, olfactory function may be affected by changes both in OC volumes, as well as intranasal, non-OC volumes [11,18,19]. Volumes anterior and inferior to the olfactory cleft have been associated with olfactory thresholds in young subjects [18]. Previous studies analysing volumetric divisions of the nasal cavity found that changes in the regions 5-10mm below the cribriform as well as

Table 4. Correlation between manual and automated measurements.

Metric	R	Sig
TotVol	0.939	p<0.001
TotOC	0.845	p<0.001
CP HU mean	0.654	p<0.001
Zygoma HU mean	0.754	p<0.001
Percentage stenosis†	0.447	p=0.002

R=Pearson correlation coefficient, Sig= significance, TotVol= total intranasal volume, TotOC=total olfactory cleft volume, †Percentage stenosis as defined by bone voxels/total voxels.

the region inferior to the olfactory cleft surrounding the head of the middle turbinate (approximately our VOI 4) to be important in olfactory function [7,8,19]. In our study, the region inferior to the olfactory cleft surrounding the middle turbinate (regions 4 and 8) demonstrated age-related changes with large effect sizes (d=0.94 and 1.09, respectively). The impact upon olfaction and confirmation with longitudinal studies remains an area for further investigation.

Marked age-related changes were also found in the bony anatomy of the cribriform plate. Previous studies have demonstrated that CT attenuation correlates with dual X-ray absorptiometry (DEXA) and that HU can serve as a surrogate measure for bone density, though it does not directly measure bone mineral content [17,21-29]. In our study, we found age-related global bone density loss as measured by mean HU, which affected the CP as well as other craniofacial bones. This age-related bone loss appears to occur diffusely throughout the CP, however, this may be more profound in the middle CP, as compared to the posterior region. As discussed in the methods, we did not analyse the anterior segment of the CP, but rather, sampled a pre-defined region of the posterior half. The anterior CP and ethmoidal foramina were shown to be thin regions with relatively large foramina in cadavers, but the effect of age-related bone density loss on this area is unclear [15].

When examining precisely how age-related bone loss occurs, it became apparent that the older cohort had a marked drop in pixels >700 HU with a corresponding increase in pixels <400 HU. Cortical bone generally has HU values >500 HU though there is no standard range accepted in current literature for cortical bone in various skeletal regions [30]. There appears to be an age-related loss of high density cortical bone with preservation of low density trabecular bone in the CP and craniofacial skeleton. This finding is consistent with previous CT demonstrations of age-related cortical bone loss in the femur [30]. Previous studies have also found age-related reduction in trabecular bone HU in the axial skeleton [25,26]. In our study, we were not able to isolate trabecular from cortical bone due to limitations in CT resolution, so it is unclear if the CP undergoes the same manner of radiographic change in aging trabecular bone.

In addition to measuring bone density, we used novel radiographic methods to measure age-related changes in olfactory foramina without relying on cadaver dissection [14]. Olfactory foramina may not always be visible on standard CTs due to slice thickness, resolution of reconstructed images and small microforamina. Calculations using CT attenuation of VOIs automates this process and theoretically overcomes many of these limitations. Additionally, CT analysis provides information as described earlier on the spectrum of bone density, while anatomic dissections simply describe the presence or absence of bone and foramina. In this study, no differences in olfactory foramina were found between age cohorts, though prior investigations in cadavers described stenosis of olfactory foramina [14]. Differences in these findings may be due to fibrous tissue or low-density bone stenosis, which may be misclassified as neural structures on CT imaging due to low HU values. Similarly, in many orthopaedic studies using CT analysis to correlate DEXA-diagnosed osteoporosis, the distribution of trabecular bone pixels—particularly in osteoporotic patients—overlapped with the upper limit of the soft tissue standard used in our study [21-23, 25, 26,29]. Our results demonstrated approximately 83-84% of the CP was bone which correlates with both clinical experience, as well as our previously published study which confirmed the accuracy of CT assessments using anatomic cadaver dissections [14].

DBM provided an alternative efficient approach for measuring nasal anatomy. There are potential uses for DBM for rhinologic research and perhaps future clinical applications. Nasal volumes were strongly correlated between manual and automated measurements. Mean cribriform HU and olfactory foramina stenosis between the methods were not as strongly correlated, which may be attributable to slight differences in the VOIs between measuring techniques. DBM allows for processing of many images at one time, which can enable future studies to include analysis of more images and anatomic regions.

Our study does have some limitations. While we found numerous age-related anatomic changes, we do not have information regarding the presence or absence of any clinical rhinologic conditions. Additionally, we selected subjects at the extremes of the spectrum of ages. Future studies are warranted examining both clinical information, as well as examining middle aged subjects to determine if there is a particular age at which some of these anatomic changes begin to appear.

Conclusion

We found that nearly all nasal airspace volumes are increased in older adults independent of sex and head size. Additionally, the cribriform plate in older adults appears to lose bone density with regional anatomic variations in bone loss. The clinical impact of these anatomic changes remains an area for further study.

Acknowledgements

This study was funded by a grant from the Centre on Aging at the Medical University of South Carolina.

Authorship contribution

RJS, ZMS, MLW, KGG and EDM contributed to the design of the work. RJS, KGG, MLW and EDM contributed to acquisition of the data and drafting of the work. All authors made substantial contributions to the analysis and interpretation of the work, revising the drafts, final approval of the manuscript, and agreed to be accountable for all aspects of the work in ensuring that questions related to the accuracy or integrity of any part of the work are appropriately investigated and resolved.

Conflict of interest

No conflicts of interest to report.

References

1. Pinto JM, Jeswani, S. Rhinitis in the geriatric population. Allergy, Asthma, Clin Immunol. 2010; 6:10
2. Rodriguez K, Rubinstein E, Ferguson BJ. Clear anterior rhinorrhoea in the population. Int Forum Allergy Rhinol. 2015; 5: 1063-1067
3. Seow Y, Ong PKC, Huang D. Odor-specific loss of smell sensitivity with age as revealed by the specific sensitivity test. Chem Senses. 2016; 41:487-495
4. Doty RL, Kamath V. The influences of age on olfaction: a review. Front Psychol. 2014 Feb 7; 5:20.
5. Renteria AE, Endam LM, Desrosiers M. Do aging factors influence the clinical presentation and management of chronic rhinosinusitis? Otolaryn Head and Neck Surg. 2012; 156(4): 598-605
6. Settipane, RA, Kaliner MA. Nonallergic rhinitis. Am J Rhinol Allergy. 2013; 27: S48-S51
7. Kalmovich LM, Elad D, Zaretsky U, Adunsky A, Chetrit A, Sadetzki S, Segal S, Wolf M. Endonasal geometry changes in elderly people: acoustic rhinometry measurements. J Gerontol. 2005; 60A (3): 396-8
8. Jun BC, Song SW, Kim BG, Kim BY, Seo JH, Kang JM, Park YJ, Cho JH. A comparative analysis of intranasal volume and olfactory function using a three-dimensional reconstruction of paranasal sinus computed tomography, with a focus on the airway around the turbinates. Eur Arch Otorhinolaryngol. 2010; 287:1389-1395
9. Garcia G, Bailie N, Martins D, Kimbell J. Atrophic rhinitis: A CFD study of air conditioning in the nasal cavity. J Appl Physiol. 2007; 103(3):1082-92
10. Lindemann J, Sannwald D, Wiesmiller K. Age-related changes in intranasal air conditioning in the elderly. Laryngoscope. 2008;118: 1472-5
11. Loftus PA, Wise SK, Nieto D, Panella N, Aiken A, DelGaudio JM. Intranasal volume increases with age: Computed tomography volumetric analysis in adults. Laryngoscope. 2016;126(10):2212-5
12. Kalmey JK TJ, Dluzen DE. Age-related size reduction of foramina in the cribriform plate. Anat Rec. 1998; Jul 25, 1(3):32-9
13. OsiriX: An Open-Source Software for Navigating in Multidimensional DICOM Images. J Digit Imaging. 2004 Sep;17(3):205-16
14. Ganjaei KG, Soler ZM, Mappus ED, Taylor RJ, Worley ML, Mulligan JK, Mattos JL, Rowan NR, Garcia GJM, Dubno JR, Eckert MA, Matthews LJ, Schlosser RJ. Novel radiographic assessment of the cribriform plate. Am J Rhinol Allergy. 2018 May;32(3):175-180.
15. Patron V, Berkaoui J, Jankowski R, Lechapt-Zalcman E, Moreau S, Hitier M. The forgotten foramina: a study of the anterior cribriform plate. Surg Radiol Anat. 2015;37(7):835–840
16. Lee IJ, Lee JJ, Bae JH, Hwang E, Lee S, Cho M, et al. Significance of osteoporosis in facial bone density using computed tomography. J Craniofac Surg. 2013;24(2):428-3
17. Blackledge MD et al., Rapid development of image analysis research tools: Bridging the gap between researcher and clinician with pyOsiriX. Comp Biol Med. 2016; 69: 203-12
18. Damm M, Vent J, Schmidt M, Theissen P, Exckel HE, Lotsch J, Hummel T. Intranasal volume and olfactory function. Chem Senses. 2002; 27: 831-9
19. Leopold DA. The relationship between nasal anatomy and human olfaction. Laryngoscope. 1988; 98:1232-8
20. Zhao K, Scherer PW, Hajiloo SA, Dalton P. Effect of anatomy on human nasal air flow and odorant transport patterns: implications for olfaction. Chem. Senses. 2004; 29:365-379
21. Lee SJ, Anderson PA, Pickhardt PJ. Predicting Future Hip Fractures on Routine Abdominal CT Using Opportunistic Osteoporosis Screening Measures: A Matched Case-Control Study. AJR Am J Roentgenol. 2017;209(2):395-402
22. Schreiber JJ, Anderson PA, Rosas HG, Buchholz AL, Au AG. Hounsfield units for assessing bone mineral density and strength: a tool for osteoporosis management. J Bone Joint Surg Am. 2011 Jun 1;93(11):1057-63.
23. Pervaiz K, Cabezas A, Downes K, Santoni BG, Frankle MA. Osteoporosis and shoulder osteoarthritis: incidence, risk factors, and surgical implications. J Shoulder Elbow Surg. 2013 Mar;22(3):e1-8.
24. Schreiber JJ, Hughes AP, Taher F, Girardi FP. An association can be found between Hounsfield units and success of lumbar spine fusion. HSS J. 2014 Feb;10(1):25-9.
25. Schreiber JJ, Anderson PA, Hsu WK. Use of computed tomography for assessing bone mineral density. Neurosurgical focus. 2014;37(1): E4.
26. Schreiber JJ, Gausden EB, Anderson PA, Carlson MG, Weiland AJ. Opportunistic osteoporosis screening - gleaning additional information from diagnostic wrist CT scans. J Bone Joint Surg Am. 2015 Jul 1;97(13):1095-100.
27. Wagner SC, Dworak TC, Grimm PD, Balazs GC, Tintle SM. Measurement of distal ulnar Hounsfield units accurately predicts bone mineral density of the forearm. J Bone Joint Surg Am. 2017;99(8):e38
28. Johnson CC, Gausden EB, Weiland AJ, Lane JM, Schreiber JJ. Using Hounsfield units to assess osteoporotic status on wrist computed tomography scans: comparison with dual energy X-ray absorptiometry. J Hand Surg Am. 2016 Jul;41(7):767-74.
29. Gausden EB, Nwachukwu BU, Schreiber JJ, Lorich DG, Lane JM. Opportunistic use of CT imaging for osteoporosis screening and bone density assessment: a qualitative systematic review. J Bone Joint Surg Am. 2017;99(18):1580-90.
30. Hoiseth A, Alho A, Husby T. Femoral cortical/cancellous bone related to age. Acta radiologica (Stockholm, Sweden:1987). 1990;31(6):626-7

Kimia Ganjaei
Rutgers Robert Wood Johnson Medical School
Piscataway, NJ 08854
United States

E-mail: kimiagrace@gmail.com